*Nano and Medical Materials 2023; 3(1): 39.*
Original Research Article

# Synthesis of MgO nanoparticles for different annealing temperatures and its biomedical applications

**Annamalai Varathan Jaya Srinivasan[1], Iruson Baskaran[1*], Balaraman Sathyaseelan[2*], Krishnamoorthy Senthilnathan[3], Elayaperumal Manikandan[4]**

*[1] Department of Physics, Arignar Anna Govt. Arts College, Cheyyar 604407, Tamil Nadu, India. E-mail: ibk1978@gmail.com*
*[2] Department of Physics, University College of Engineering Arni (A Constituent College of Anna University Chennai), Arni 632326, Tamil Nadu, India. E-mail: bsseelan.tvu@gmail.com*
*[3] Department of Physics, VIT University, Vellore 632014, Tamil Nadu, India.*
*[4] Departmentof Physics, Thiruvalluvar University, TVUCAS Campus, Thennangur 604408, Tamil Nadu, India.*

**ARTICLE INFO**

Received: 10 March 2023
Accepted: 25 April 2023
Available online: 26 May 2023

http://dx.doi.org/10.59400/nmm.v3i1.39



**ABSTRACT:** In this paper, we report the synthesis of MgO nanoparticles (NPs) by the co-precipitation method. The structural properties of the samples were characterised by X-ray diffraction, which revealed that the MgO Nps have a cubic structure. The functional groups of the as-synthesised samples were analysed by Fourier transform infrared spectroscopy. The optical properties of the as-synthesised samples were studied by UV-vis spectroscopy in the range of 200–800 nm, and the energy bandgap was calculated by the taus relation. The magnesium oxide (MgO) nanoparticles (NPs) showed significant dose-dependent bactericidal activity in both gram-negative and gram-positive bacteria. From the analysis of the antibacterial and antifungal activities of MgO NPs, it is revealed that the dose is sufficient for killing. These may be used in medical applications.

***KEYWORDS:*** magnesium oxide; co-precipitation; antibacterial; antifungal activity; phase-transformation

## 1. Introduction

In the last decade, great attention has been paid to nanosized materials because of their unusual physical, chemical properties[1–3]. Magnesium oxide (MgO) is an alkaline earth metal oxide that has a rock salt structure and a large band gap of 4.5 eV. MgO has many properties. For example, in biomedical applications, its high specific surface area is responsible for the antibacterial activity of the microorganism[4–6]. MgO NPs samples have antibacterial activity in addition to their physicochemical characteristics. The antibacterial activity of MgO NPs lies in the fact that they generate superoxide radicals by reaching oxygen on the bacterial cell surface. The superoxide radical has extra electrons and is very reactive[7,8]. Especially analysts have observed the synthesis of MgO nanoparticles because of their outlandish applications. MgO nanoparticles are the most important in several fields, such as superconducting, pH regulator for wastewater treatment, catalyst[9,10], remediation of chemical waste and warfare agents[11], electronics, cosmetics[12], reflecting and anti-reflecting coatings and coating agents[13,14], plasma display panels, heat-insulating, refractory fiber board, high-frequency magnetic rod antenna dehydrating agent used, electrically insulating material for making crucibles, and antibacterial material for waste remediation and superconductor products[15,16]. MgO nanoparticles have been recasting fields like industries, medicine, and microelectronics[12]. It is a semiconducting material with a

band gap that is used in the production of next-generation solar cells[17,18]. The pure MgO nanoparticles exhibit moderate acidity but have strong basicity[19]. Also, due to its large specific surface area, it has good photocatalytic properties[20,21]. Antimicrobial activities against different pathogens have been studied[22–25]. Fungi are the most dangerous for paper objects and cultural heritage[26]. Magnesium oxide is a naturally occurring compound discovered in seawater and metamorphic rocks[27,28]. The magnesium oxide has a high melting point of 3,125 K and a high boiling point of 3,873 K. Due to this, it has higher electrical resistivity, chemical stability, and thermal expansion coefficient.

Various techniques have been implemented to produce various kinds of MgO NPs by different synthesis processes, such as sol-gel method[29–33], flame spray pyrolysis method[34], microwave-assisted sol-gel synthesis[6,35], sonochemical[36], hydrothermal[37], chemical vapour deposition (CVD)[38], pulsed laser deposition (PLD)[39], green synthesis[12], method of surface preparation[40], and co-precipitation method[41,42]. The co-precipitation technique is the most advantageous technique in the synthesis of nanomaterials and nanoparticles because it has a very simple technique, a low cost, and a low crystallisation temperature.

In this work, we developed MgO nanoparticles by the co-precipitation method and reported the characterization of MgO for different calcinations. By using CuKα radiation in an X-ray diffractometer, the behaviour of phase formation and the nature of the crystallinity of the sample are recognised. The optical properties and energy band gap values are recognised by the UV-Vis spectrometer. The presence of functional groups was identified by the Fourier transform infrared spectrometer (FTIR). Surface morphologies of nanopowder have been studied using field emission scanning electron microscope (FESEM) images, and their potential antimicrobial activity against *Aspergillus niger*, *Aspergillus flavus*, and *Candida albicans* has been reported.

## 2. Experimental method

To synthesise MgO NPs, it is done by the co-precipitation method by using 0.01 M of magnesium nitrate ($Mg(NO_3)2.6H_2O$) and 0.02 M of sodium hydroxide (NaOH) in deionized water to make a homogenous solution. Then the NaOH solution was dropwise mixed with the magnesium nitrate solution under continuous stirring for 6 h. The mixture was ultrasonicated for 3 h at room temperature and allowed one day to settle. The prepared sample was completely washed with distilled water and filtered. The filtered sample was dried for 48 h at 80 °C and annealed at different temperatures of 200 °C, 400 °C, and 60 °C for 1 h.

### 2.1 Characterization

The crystal structure of synthesized MgO nanoparticle samples was carried out with the aid of a GNR APD PRO 2000 X-ray diffractometer (XRD) with a step size of 0.05°/min in the 2θ range 20–90°. CuKα radiation (Å) was used as a source. FTIR analysis of the samples was done by Thermo Scientific Nicolet IS10 IR spectrometer, and UV visible measurements of the samples were performed with a Shimadzu UV-vis 2600 UV spectrometer. Field emission scanning electron microscopy (FESEM) was recorded using a Carl Zeiss Merlin compact microscope. MgO nanoparticles were analysed by thermal analysis using the TGA instrument of the EXSTAR 6200, which gives a thermogravimetric curve fitted with a differential thermal analyzer simultaneously from room temperature to 800 °C.

### 2.2 Antimicrobial assay

The minimum inhibitory concentration (MIC) of NPs was tested in *S.faecalis, B.subtilis, S.aureus,* and *E.coli* by the micro-agar dilution method. A stock solution of the MgO NPs was prepared by dissolving 5 mg of the compound in 1 mL of distilled water and sonicating. The agar medium containing the NPs at a final concentration of 150 mg/mL was poured into Petri dishes,

swirled gently until the agar began to set, and left overnight for solvent evaporation. Microorganisms were streaked in a radial pattern on the agar plates, and the inoculum of each test strain was standard-sized at $5 \times 10^5$ CFU/mL using canonical library standards. The plates were incubated under aerobic conditions at 37 °C for 24 h. After the incubation period, the average concentration of the test compounds, which apparently caused complete inhibition of the growth of the organism, was taken as the MIC. The bare MgO NPs were also tested for comparison.

# 3. Results

## 3.1 XRD studies

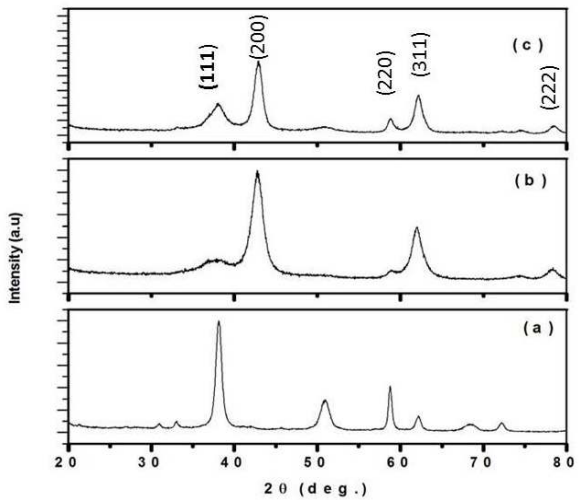


**Figure 1.** XRD patterns of MgO nanoparticles annealed at different temperatures (a) 200 °C, (b) 400 °C, and (c) 600 °C.

**Figure 1** shows the XRD patterns of MgO NPs. The diffraction peaks of MgO NPs can be indexed to the (111), (200), (220), (311), and (222) planes. The obtained diffraction peaks are in good agreement with the standard XRD data for the cubic phase of the MgO JCPDS Card (No. 87–0653)[15]. In **Figure 1(a)**, some secondary characteristic peaks of $Mg(OH)_2$, Mg, or other impurities were detected in the XRD pattern. Debye Scherrer's formula Eq (1) was used to evaluate the crystallite size for MgO.

$$D = \frac{K\lambda}{\beta cos\theta} \quad (1)$$

where $D$ is the particle size, $\lambda$ is the wavelength of the X-ray, $\beta$ is full with half maximum (FWHM), and $\theta$ is the Braggs angle. The average crystallite size of the prepared samples was found to be 12 nm, 14 nm, and 7 nm, respectively.

## 3.2 FESEM studies

**Figure 2** exhibits the FESEM images of MgO NPs. The particles appear the same spherical form agglomerated and the grain size of the particles is in the range of 50–60 nm[43]. Annealing results in further agglomeration of the particle, as well as deterioration of flake-like shaped nanoparticles of magnesium, can be seen.

## 3.3 Thermal studies

**Figure 3** shows the thermal gravimetric analysis (TGA) of the MgO NPs samples. The weight loss of the samples can be clearly ascribed to two reactions which are degradation in stages 1 and 2. The degradation in first weight loss occurs in the temperature range of 150 °C to 240 °C, an endothermic peak due to the removal of crystallizing water. This weight loss is 6.94% which agrees very well with the weight loss in a chemical reaction. In the second degradation, weight loss of about 31.8% was observed at the temperature of 250 °C to 500 °C accompanied by a broad endothermic peak of approximately 480 °C can be ascribed to the decomposition of the product of MgO NPs. The MgO NPs samples to the TGA show a horizontal line after 500 °C indicating that the MgO stable phase is formed at this temperature. Differential scanning calorimetry (DSC) profile showed the thermal decomposition is accompanied by the release of heat energy as can be observed by the endothermic peaks at 380 °C respectively shown in the DSC curve[44].

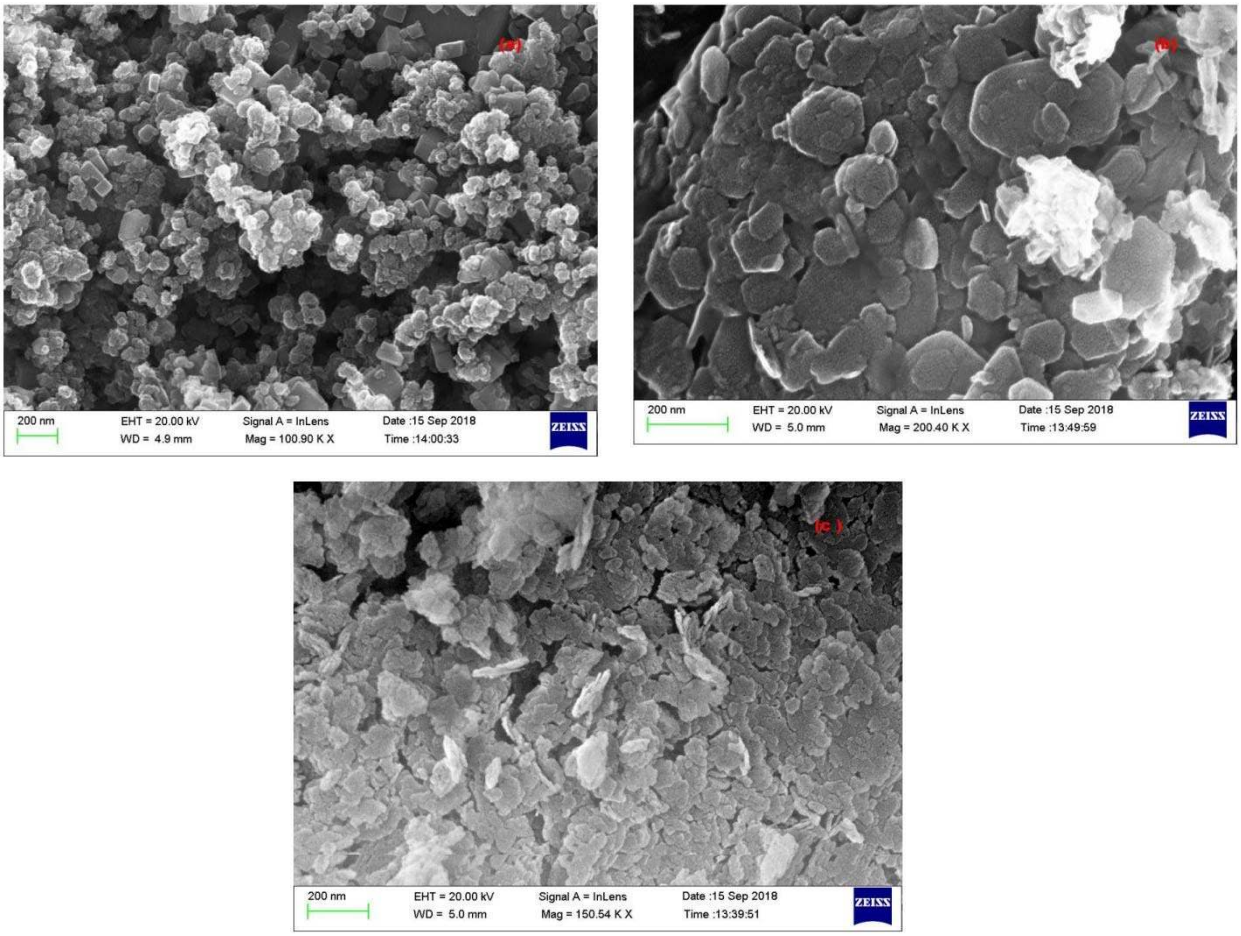


**Figure 2.** FESEM images of MgO nanoparticles annealing at different temperatures (a) 200 °C, (b) 400 °C, and (c) 600 °C.

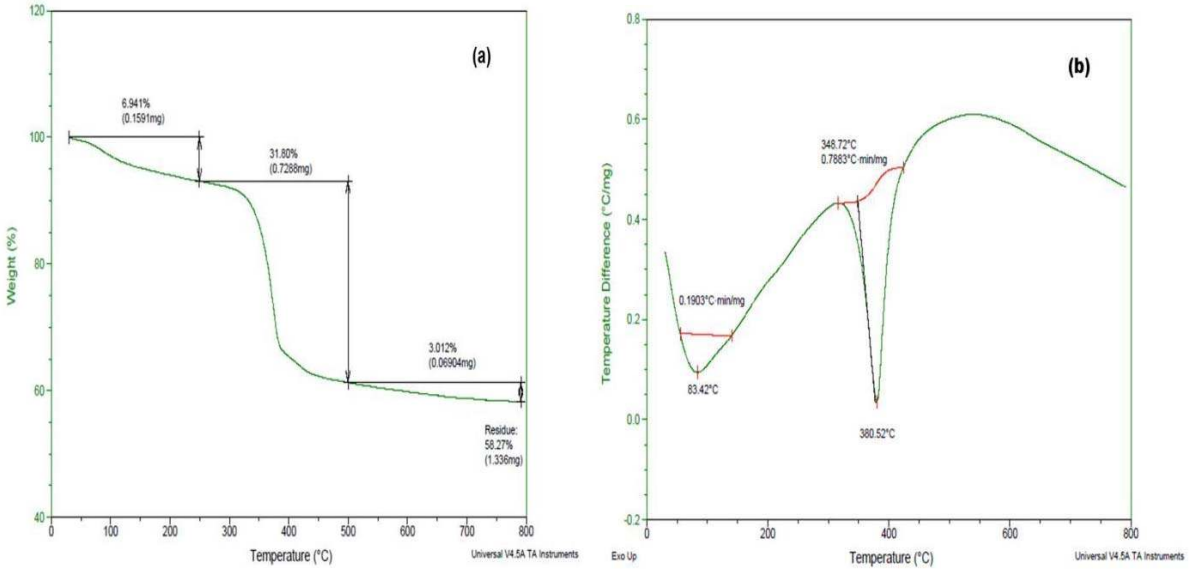


**Figure 3.** (a) TGA curve of MgO nanoparticles; (b) DSC curve of MgO nanoparticles.

## 3.4 FTIR studies

**Figure 4** shows the FTIR spectra of MgO NPs. The bands at 3,000 $cm^{-1}$–3,700 $cm^{-1}$ with the absorption peak at 3,433 $cm^{-1}$ and 3,696 $cm^{-1}$ attributed to the O-H stretching vibration[45,46].

The peaks present at 2,922 $cm^{-1}$ and 2,857 $cm^{-1}$ are attributed to C-H stretching mode bonds. The peak present at 1,630 $cm^{-1}$ is N-H bending band. The peaks at 1,481 $cm^{-1}$ and 1,422 $cm^{-1}$ are represented by C-C bonds. The strong bonds at 569 $cm^{-1}$ and 437 $cm^{-1}$ were related to the characteristics of stretching vibration in MgO[47].

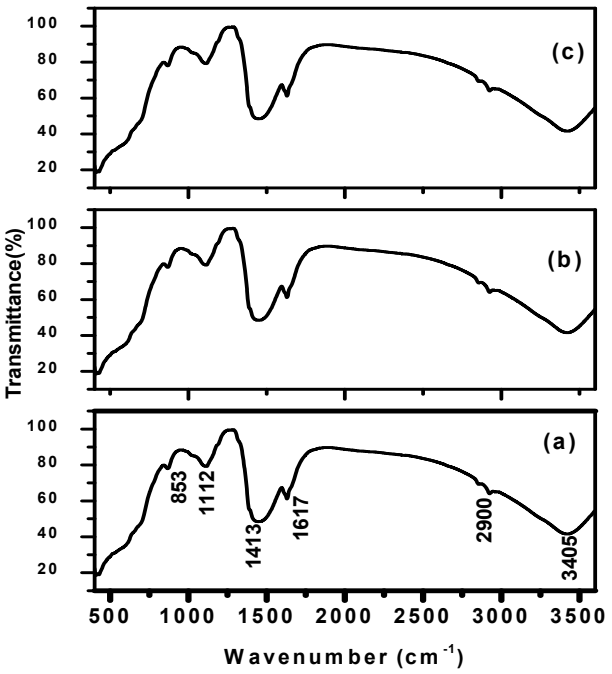


**Figure 4.** FTIR spectra of MgO nanoparticles (a) 200 °C, (b) 400 °C and (c) 600 °C.

## 3.5 UV-visible spectrocopy and tauc's plot

The absorption spectrum of MgO NPs is depicted in **Figure 5**. The absorption peak was observed at 367 nm (**Figure 5(a)**). This is very close to the reported value of 368 nm[48]. **Figure 5(b)** shows the location of the absorption peaks which is 220–800 nm. Also, no more sharp peaks are in the graph that indicates the presence of different sizes of the particles.

The energy gap of the sample is estimated by Tauc's plots fig using the following Tauc's Eq (2).

$$\alpha h\nu = A(h\nu - E_g)^n \quad (2)$$

the absorption coefficient, A is the constant, h is the plank's constant, ν is the frequency, $E_g$ is the optical band gap energy, and n is equal to ½ for the direct allowed transition. From **Figure 5(b)**, $E_g$ can be estimated as the linear region of hν Vs $(\alpha h\nu)^2$ on the X-axis. The intercept of the extra plotted straight line portion of the curves at zero absorption coefficient values gives the energy band value. From the Taucs plot, the energy band gap of MgO NPs was about 5.79 eV, 5.96 eV and 5.93 eV were smaller than the energy band gap of bulk MgO (7.8 eV)[49]. The difference in bandgap energy between NPs and bulk materials may be attributed to the planer defect[50].

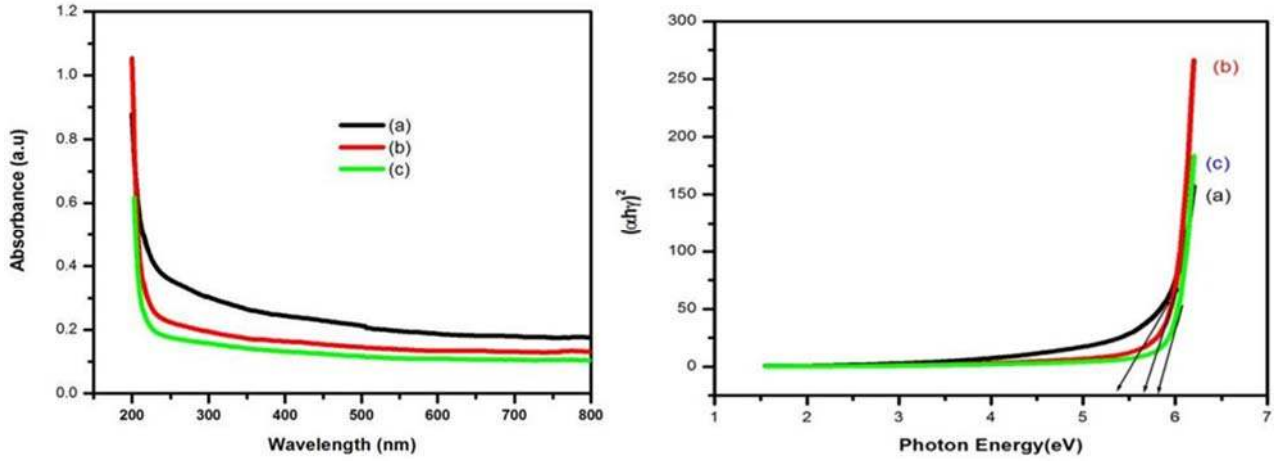


**Figure 5.** (a) UV–Vis spectra of MgO nanoparticles annealed at different temperatures along with their (b) Tauc plots.

## 3.6 Antibacterial activity

Antibacterial activity of the MgO NPs was investigated against various bacterial strains, including *Enterococcus faecalis*, *Bacillus subtitles*, *staphylococcus Aureus* and *Escherichia coli* in a good diffusion assay method. The zone of inhibition values of each bacterial agent against the test bacterial strain is provided in **Table 1**. The antibacterial activity of **Figure 6** exhibited maximum zone inhibition against a range of bacteria. It revealed that the MgO NPs were spherical and small in diameter (15–30 nm) and exhibited antibacterial activity. Even though the appropriate antibacterial mechanism of nanoparticles is unknown, it is evident that the morphology or high surface area of MgO NPs is important for many food and pharmaceutical applications.

**Table 1**. Anti-bacterial activities MgO nanoparticles

| S. No. | Microorganisms | Control | MG2 | MG4 | MG6 | Ciprofloxacin |
|---|---|---|---|---|---|---|
| | | Zone of inhibition (mm) | | | | |
| 1. | *Enterococcus faecalis* | – | – | – | – | 30 |
| 2. | *Escherichia coli* | – | – | – | – | 28 |
| 3. | *Bacillus subtilis* | – | – | – | – | 18 |
| 4. | *Staphylococcus aureus* | – | – | – | – | 15 |

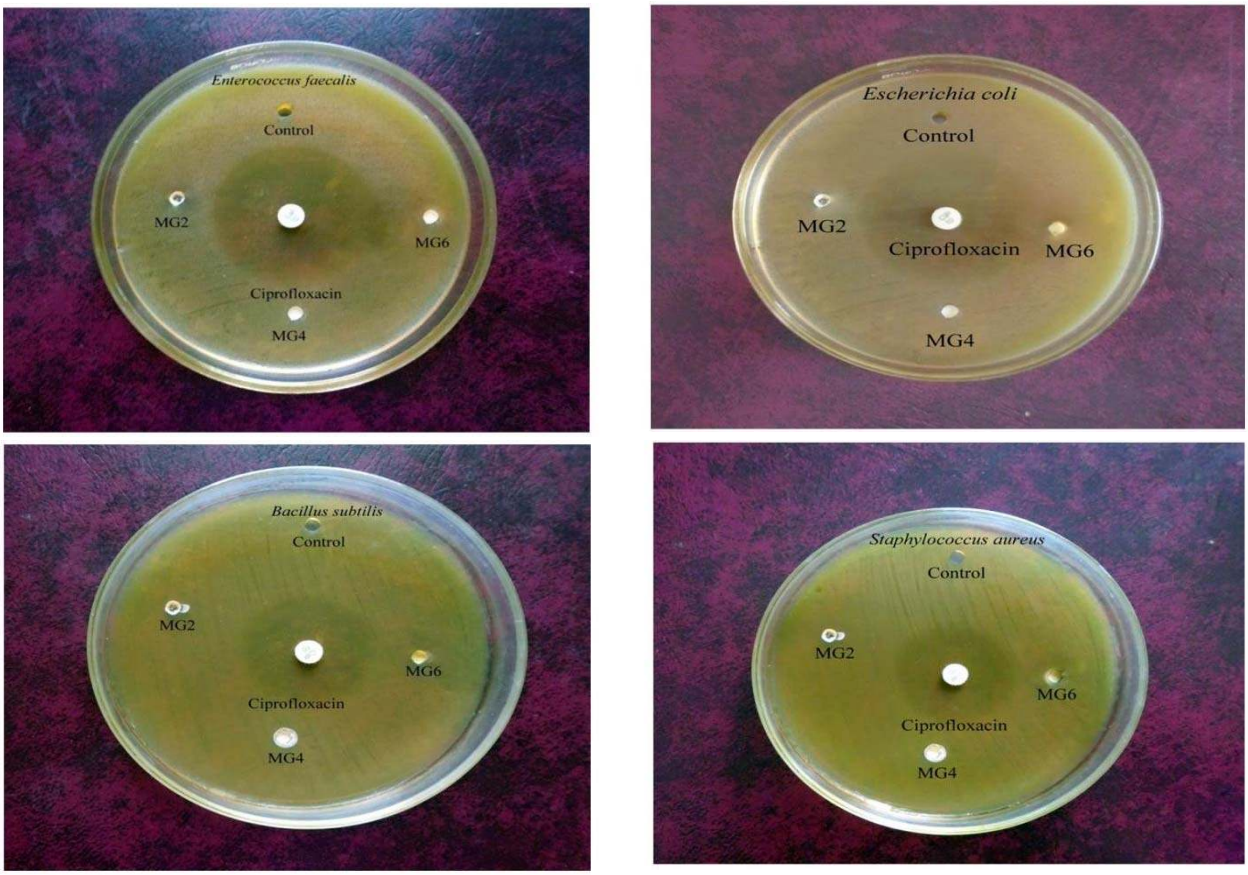


**Figure 6.** Anti-bacterial activities of MgO nanoparticles.

The formula for the activity index is calculated by comparing the inhibition zones of nanoparticles[51– 53].

$$Activity\ Index = \frac{Inhibitions\ Zone\ by\ the\ NP\ sample}{Inhibitions\ zone\ by\ the\ standard}$$

## 3.7 Antifungal activities

The antifungal activity of MgO NPs was first determined by the agar diffusion method in terms of the zone of inhibition of fungal growth. **Figure 7** shows the antifungal activity against *A. Niger*, *A. Flavus*, and *C. Albicans* fungus. The diameter of the inhibition zone in the presence of NPs is presented in **Table 2**. These results showed that MgO NPs exhibited excellent antifungal activity in all cases, presenting maximum activity in *A. Nigar* by contrast, *A. Flavus* and *C. Albicans* did not present an inhibition zone against the fungi test in all cases[54]. Therefore, MgO NPs can be generally utilised in healing and biomedical treatments, dental insets, paints in clinical and hospital rooms, and as construction materials.

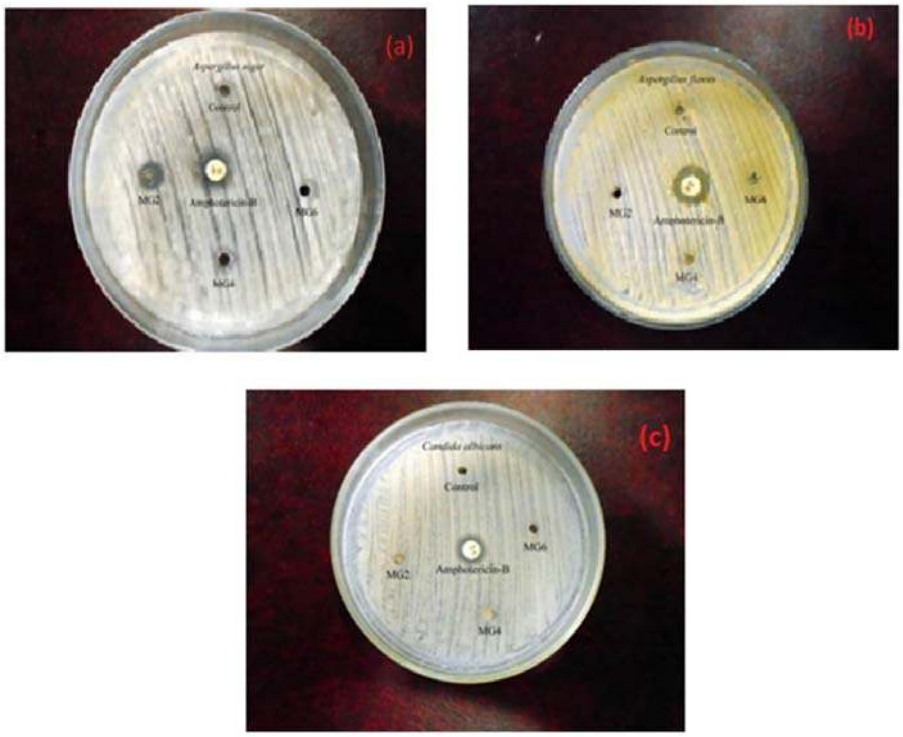


**Figure 7.** Anti-fungal activities of MgO nanoparticles.

**Table 2.** Anti-fungal activities MgO nanoparticles

| S. No. | Microorganisms | Control | MG2 | MG4 | MG6 | Amphotericin-B |
|---|---|---|---|---|---|---|
| | | Zone of inhibition (mm) | | | | |
| 1. | *Aspergillus niger* | – | 8 | 5 | 5 | 13 |
| 2. | *Aspergillus flavus* | – | – | – | – | 12 |
| 3. | *Candida albicans* | – | – | – | – | 7 |

# 4. Discussion

## 4.1 XRD analysis of MgO NPs

The average crystalline size of the MgO-NPs samples based on the values was determined to be 12 nm, 14 nm, and 7 nm, respectively. In the crystallisation of the samples, centrifugation and particle dispersion in water followed the formation of nanoparticles. Also, the expansion of peaks in the stable XRD pattern is due to the influence of particle size.

## 4.2 FESEM studies of MgO NPs

The aggregation of particles may be due to Van der Waal forces and interactions between magnesium oxide nanoparticles[55]. All of the nanoparticles are in the range between 50 and 60 nm (**Figure 2**). The average size of the MgO NPs was calculated to be 20 nm. The surface morphology presented has beneficial applications in catalysis[56] and medicine[57].

## 4.3 Thermal analysis of MgO NPs

The thermal analysis of the dried MgO NPs sample is performed by monitoring its weight loss when subjected to the increasing temperature at a rate of 20 ºC/min up to 1,000 ºC under inert conditions. The TGA curves obtained for all the samples are analysed, and it can be observed that there is a thermal decomposition of the MgO NPs samples. It can be observed from **Figure 2** that, the degradation in the first stage occurs in the temperature range of 40–200 ºC and annealing of the MgO powder sample at the melting transition temperature yields nanosized powders of MgO.

## 4.4 FTIR spectroscopic analysis of MgO NPs

Because of the presence of alcoholic groups, a large peak can be seen in the area between 3,400 and 3,300 $cm^{-1}$ in **Figure 4(a–c)**. The infrared band at 3,356 $cm^{-1}$ was shown in **Figure 4**. For the O-H bond vibrations of a hydroxy group, a slight decrease in peak intensity, and a shift of the peak from 3,433 $cm^{-1}$ to 3,696 $cm^{-1}$ in **Figure 4** indicate the role of organic molecules in the development of MgO nanoparticles. This broad peak at 3,696 $cm^{-1}$ helps stabilise the particle crystal growth while restricting the particle size and preventing agglomeration. The peak at 2,922 $cm^{-1}$ suggests the stretching of alkynes. The absorption peak at 1,481 $cm^{-1}$ and 1,422 $cm^{-1}$ was subjected to C-H bending vibrations of an aromatic tertiary amine group. The peaks observed at 569 and 437 $cm^{-1}$ indicate the formation of MgO NPs. Such peaks are observed due to vibrations of magnesium oxide. Likewise, MgO nanoparticles synthesized by Tamilselvi[45] generated large FTIR transmission peaks at 437 and 569 $cm^{-1}$, due to the presence of magnesium oxide vibrations.

## 4.5 UV spectroscopy analysis of MgO NPs

A single peak appearance in the UV-spectrum of MgO NPs shows that the prepared NPs are isomorphological. As shown in **Figure 5**, the absorption peak lies in the range of 200–800 nm. In this process, the lack of sharp peaks indicates the synthesis of nanoparticles at different sizes and supports the findings of the ultraviolet-visible spectrum and electron microscopy.

## 4.6 Minimum inhibitory concentration MgO NPs

In antibacterial activity against *Enterococcus faecalis*, *Bacillus subtitles*, *Staphylococcus Aureus* and *Escherichia coli* studies by Chung *et al*.[46] showed that tannins from different structures prevented the growth of the microorganism. Flavonoids have been documented as having both antibacterial and antifungal activity against *Enterococcus faecalis*, *Bacillus subtitles*, *Staphylococcus Aureus* and *Escherichia coli*. The magnesium oxide nanoparticles have probably shown significant antibacterial activity against *E.coli* and *S.aureus* because the MgO NPs can easily reach the nucleus of the bacteria and provide an excellent surface area for interactions that impede development. In this study, we have reported the efficacy of MgO NPs and other metallic nanoparticles on antibacterial behaviour based on the occurrence of oxygen vacancies on the surface of the nanoparticles. Increased pH and $Mg^{2+}$ ions have been predicted to play an important role in the mode of action of MgO nanoparticles against microbes, provided that MgO nanoparticles dissociate in microbial culture and release OH-ions and $Mg^{2+}$ ions[58]. Initial studies of metallic nanoparticles' antimicrobial activities showed huge potential in the food industry, biomedical science, and many other science and technology sectors because these substances can offer enduring antibacterial activities due to their intrinsic instability and high-temperature tolerance properties[59]. Metallic nanocomponent alternatives are important to significantly increase the magnitude and incidence of multidrug-resistant bacterial strains[60].

MgO NPs exhibited the maximal inhibition zone found in **Tables 1** and **2**. MgONPs, strong in electrostatic association with the bacterial surface, contributed to cell death[61,62].

## 5. Conclusion

The synthesis of MgO NPs was successfully done by the co-precipitation technique. MgO NPs were annealed in air at 200 °C, 400 °C, and 600 °C. The X-ray diffraction pattern indicates that the obtained nanoparticles are well crystalline, and a morphological investigation by SEM reveals the typical cubic shape. The signature of functional groups present in MgO NPs is shown by FTIR spectra. The MgO NPs exhibited antibacterial activity against the growth of microorganisms. The MIC of the existing bacterial strains was also determined.

## Conflict of interest

The authors declare no competing conflict of interest.

## References


1. Sekar P, Narendranath S, Desai V. Recent progress in *in vivo* studies and clinical applications of magnesium based biodegradable implants—A review. Journal of Magnesium and Alloys 2021; 9(4): 1147–1163. doi: 10.1016/j.jma.2020.11.001.
2. Nie Y, Dai J, Li X, Zhang X. Recent developments on corrosion behaviors of Mg alloys with stacking fault or long period stacking ordered structures. Journal of Magnesium and Alloys 2021; 9(4): 1123–1146. doi: 10.1016/j.jma.2020.09.021.
3. Molaei M, Babaei K, Fattah-alhosseini A. Improving the wear resistance of plasma electrolytic oxidation (PEO) coatings applied on Mg and its alloys under the addition of nano- and micro-sized additives into the electrolytes: A review. Journal of Magnesium and Alloys 2021; 9(4): 1164–1186. doi: 10.1016/j.jma.2020.11.016.
4. Wang C, Kang J, Deng K, *et al*. Microstructure and mechanical properties of Mg-4Zn-xGd (x=0, 0.5, 1, 2) alloys. Journal of Magnesium and Alloys 2020; 8(2): 441–451. doi: 10.1016/j.jma.2019.06.005.
5. Ariga K, Yamauchi Y, Aono M. Commentary: Nanoarchitectonics—Think about NANO again. APL Materials 2015; 3(6): 061001. doi: 10.1063/1.4922549.
6. Bdewi SF, Abdullah OG, Aziz BK, Muta AAR. Synthesis, structural and optical characterization of MgO nanocrystalline embedded in PVA matrix. Journal of Inorganic and Organometallic Polymers and Materials 2016; 26: 326–334. doi: 10.1007/s10904-015-0321-3.
7. Tamilselvi P, Yelilarasi A, Hema M, Anbarasan R. Synthesis of hierarchical structured MgO by sol-gel method. Journal of Nanotechnology Bulletin 2013; 2(1): 130106–1301065. doi: 10.1234/NANO130106.
8. Guan H, Wang P, Zhao B, *et al*. Synthesis of high surface area nanometer magnesia by solid-state chemical reaction. Frontiers of Chemistry in China 2007; 2: 204–208. doi: 10.1007/s11458-007-0041-5.
9. Niu H, Yang Q, Tang K, Xie Y. Large-scale synthesis of single-crystalline MgO with bone-like nanostructures. Journal of Nanoparticle Reasearch 2006; 8: 881–888. doi: 10.1007/s11051-006-9138-x.
10. Yuan G, Zheng J, Lin C, *et al*. Electrosynthesis and catalytic properties of magnesium oxide nanocrystals with porous structures. Materials Chemistry and Physics 2011; 130(1–2): 387–391. doi: 10.1016/j.matchemphys.2011.06.058.
11. Wagner GW, Bartram PW, Koper O, Klabunde KJ. Reactions of VX, GD, and HD with nanosize MgO. The Journal of Physical Chemistry B 1999; 103(16): 3225–3228. doi: 10.1021/jp984689u.
12. Moorthy SK, Ashok CH, Venkateswara Rao V, Viswanathan C. Synthesis and characterization of Mgo nanoparticles by neem leaves through green method. Materials Today: Proceedings 2015; 2(9): 4360–4368. doi: 10.1016/j.matpr.2015.10.027.
13. Park JS, Han YH. Effects of MgO coating on microstructure and dielectric properties of $BaTiO_3$. Journal of the European Ceramic Society 2007; 27(2–3):1077–1082. doi: 10.1016/j.jeurceramsoc.2006.05.073.
14. Salem JK, El-Nahhal IM, Hammad TM, *et al*. Optical and fluorescence properties of MgO nanoparticles in micellar solution of hydroxyethyl laurdimonium chloride. Chemical Physics Letters 2015; 636: 26–30. doi: 10.1016/j.cplett.2015.07.014.
15. Najafi A. A novel synthesis method of hierarchical mesoporous MgO nanoflakes employing carbon nanoparticles as the hard templates for photocatalytic degradation. Ceramics Interna-

tional 2017; 43(7): 5813–5818. doi: 10.1016/j.ceramint.2017.01.135.

16. Sutradhar N, Sinhamahapatra A, Pahari SK, *et al*. Controlled synthesis of different morphologies of MgO and their use as solid base catalysts. The Journal of Physical Chemistry C 2011; 115(25): 12308–12316. doi: 10.1021/jp2022314.

17. Huang CH, Jan YL, Lee WC. Investigation of Mg(O,OH) films prepared by chemical bath deposition as buffer layers for Cu(In,Ga)$Se_2$ solar cells. Journal of the Electrochemical Society 2011; 158(9): H879. doi: 10.1149/1.3609047.

18. Das PS, Dey A, Mandal AK, *et al*. Synthesis of $Mg(OH)_2$ micro/nano flowers at room temperature. Journal of Advanced Ceramics 2013; 2(2): 173–179. doi: 10.1007/s40145-013-0058-9.

19. Tanabe K. Solid acids and bases: Their catalytic properties. New York: Academic Press; 1970. doi: 10.1016/B978-0-12-683250-1.X5001-9.

20. Borhede AV, Kanade KG, Tope DR, Patil MD. A comparative study on synthesis, characterization and photocatalytic activities of MgO and Fe/MgO nanoparticles. Research on Chemical Intermediates 2012; 38(8): 1931–1946. doi: 10.1007/s11164-012-0515-z.

21. Anpo M, Moon SC, Chiba K, *et al*. Intrinsic surface structures and their roles in the catalysis and photo-catalysis of microcrystalline MgO catalysts. Research on Chemical Intermediates 1993; 19(6): 495–519. doi: 10.1163/156856793X00451.

22. Stoimenov PK, Klinger RL, Marchin GL, Klabunde KJ. Metal oxide nanoparticles as bactericidal agents. Langmuir 2002;18(17): 6679–6686. doi: 10.1021/la0202374.

23. Makhluf S, Dror R, Nitzan Y, *et al*. Microwave-assisted synthesis of nanocrystalline MgO and its use as a bacteriocide. Advanced Functinal Materials 2005; 15(10): 1708–1715. doi: 10.1002/adfm.200500029.

24. Das B, Moumita S, Ghosh S, *et al*. Biosynthesis of magnesium oxide (MgO) nanoflakes by using leaf extract of Bauhinia purpurea and evaluation of its antibacterial property against Staphylococcus aureus. Materials Science and Engineering: C 2018; 91: 436–444. doi: 10.1016/j.msec.2018.05.059.

25. Sawai J, Kojima H, Igarashi H, *et al*. Antibacterial characteristics of magnesium oxide powder. World Journal of Microbiology and Biotechnology 2000; 16(2): 187–194. doi: 10.1023/A:1008916209784.

26. Coutinho ML, Miller AZ, Phillip A, *et al*. Biodeterioration of majolica glazed tiles by the fungus Devriesia imbrexigena. Construction and Building Materials 2019; 212: 49–56. doi: 10.1016/j.conbuildmat.2019.03.268.

27. Amaral LF, Oliveira IR, Salomao R, *et al*. Temperature and common-ion effect on magnesium oxide (MgO) hydration. Ceramics International 2010; 36(3): 1047–1054. doi: 10.1016/j.ceramint.2009.12.009.

28. Hall RJ, Spencer DRF. A review of the production and properties of sea-water magnesia. Interceram 1973; 22: 212–218.

29. Mastuli MS, Kamarulzaman N, Nawawi MA, *et al*. Growth mechanisms of MgO nanocrystals *via* a sol-gel synthesis using different complexing agents. Nanoscale Research Letters 2014; 9: 134. doi: 10.1186/1556-276X-9-134.

30. Mehta M, Mukhopadhyay M, Christian R, Mistry N. Synthesis and characterization of MgO nanocrystals using strong and weak bases. Powder Technology 2012; 226: 213–221. doi: 10.1016/j.powtec.2012.04.044.

31. Bokhimi, Morales A, Lopez T, Gomez R. Crystalline structure of MgO prepared by the sol-gel technique with different hydrolysis catalysts. Journal of Solid State Chemistry 1995; 115(2): 411–415. doi: 10.1006/jssc.1995.1152.

32. Ma J, Chen CZ, Wang DG, Hu JH. Synthesis, characterization and in vitro bioactivity of magnesium-doped sol-gel glass and glass-ceramics. Ceramics International 2011; 37(5): 1637–1644. doi: 10.1016/j.ceramint.2011.01.043.

33. Portillo R, Lopez T, Gomez R, *et al*. Magnesia synthesis via sol-gel: Structure and reactivity. Lengmuir 1996; 12(1): 40–44. doi: 10.1021/la940694n.

34. Demirci S, Ozturk B, Yildirim S, *et al*. Synthesis and comparison of the photocatalytic activities of flame spray pyrolysis and sol–gel derived magnesium oxide nano-scale particles. Materials Science in Semiconductor Processing 2015; 34: 154–161. doi: 10.1016/j.mssp.2015.02.029.

35. Mirzaei H, Davoodnia A. Microwave assisted sol-gel synthesis of MgO nanoparticles and their catalytic activity in the synthesis of hantzsch 1,4-dihydropyridines. Chinese Journal of Catalysis 2012; 33(9–10): 1502–1507. doi: 10.1016/S1872-2067(11)60431-2.

36. Alavi MA, Morsali A. Syntheses and characterization of $Mg(OH)_2$ and MgO nanostructures by ultrasonic method. Ultrasonics Sonochemistry 2010; 17(2): 441–446. doi:

10.1016/j.ultsonch.2009.08.013.

37. Wang JA, Novaro O, Bokhimi X, *et al*. Characterizations of the thermal decomposition of brucite prepared by sol-gel technique for synthesis of nanocrystalline MgO. Materials Letters 1998; 35(5–6): 317–323. doi: 10.1016/S0167-577X(97)00273-5.

38. Li H, Li M, Wang X, *et al*. Synthesis and optical properties of single-crystal MgO nanobelts. Materials Letters 2013; 102–103: 80–82. doi: 10.1016/j.matlet.2013.03.118.

39. Nagashima K, Yanagida T, Tanaka H, Kawai T. Epitaxial growth of MgO nanowires by pulsed laser deposition. Journal of Applied Physics 2007; 101(12): 124304. doi: 10.1063/1.2748625.

40. Perry SS, Merrill PB. Preparation and characterization of MgO(100) surfaces. Surface Science 1997; 383 (2–3): 268–276. doi: 10.1016/S0039-6028(97)00185-4.

41. Henrist C, Mathieu JP, Vogels C, *et al*. Morphological study of magnesium hydroxide nanoparticles precipitated in dilute aqueous solution. Jouranl of Crystal Growth 2003; 249(1–2): 321–330. doi: 10.1016/S0022-0248(02)02068-7.

42. Fedorov PP, Tkachenko EA, Kuznetsov SV, *et al*. Inorganic Materials 2007; 43: 502–504. doi: 10.1134/S0020168507050111.

43. Cvetkovic VS, Vukicevic NM, Nikolic ND, *et al*. Formation of needle-like and honeycomb-like magnesium oxide/hydroxide structures by electrodeposition from magnesium nitrate melts. Electrochimica Acta 2018; 268: 494–502. doi: 10.1016/j.electacta.2018.02.121.

44. Yang W, Zhu Z, Shi J, *et al*. Characterizations of the thermal decomposition of nano-magnesium hydroxide by positron annihilation lifetime spectroscopy. Powder Technology 2017; 311: 206–212. doi: 10.1016/j.powtec.2017.01.059.

45. Tamilselvi P, Yelilarasi A, Hema M, Anbarasan R. Synthesis of hierarchical structured MgO by sol-gel method. Nano Bulletin 2013; 2: 130106. doi: 10.1234/NANO130106.

46. Chung KT, Wong TY, Wei CI, *et al*. Tannins and human health: A review. Critical Reviews in Food Science and Nutrition 1998; 38(6): 421–464. doi: 10.1080/10408699891274273.

47. Nigam A, Saini S, Rai AK, Pawar SJ. Structural, optical, cytotoxicity, and antimicrobial properties of MgO, ZnO and MgO/ZnO nanocomposite for biomedical applications. Ceramics International 2021; 47(14): 19515–19525. doi: 10.1016/j.ceramint.2021.03.289.

48. Pandey R, Jaffe JE, Kunz AB. Ab initio band-structure calculations for alkaline-earth oxides and sulfides. Physical Review B 1991; 43(11): 9228. doi: 10.1103/PhysRevB.43.9228.

49. Bindhu MR, Umadevi M, KavinMicheal M, *et al*. Structural, morphological and optical properties of MgO nanoparticles for antibacterial applications. Materials Letters 2016; 166: 19–22. doi: 10.1016/j.matlet.2015.12.020.

50. Islam I, Siddiqui AM, Hafiz AK, *et al*. Influence of pH and Fe doping on structural and physical properties of $Mg_{0.95}Mn_{0.05-x}Fe_xO$ ($x$ = 0,0.04) nanoparticles. Journal of Physics and Chemistry of Solids 2019; 133: 197–202. doi: 10.1016/j.jpcs.2019.05.030.

51. Bindhu MR, Umadevi M. Antibacterial activities of green synthesized gold nanoparticles. Materials Letters 2014; 120: 122–125. doi: 10.1016/j.matlet.2014.01.108.

52. Jin T, He Y. Antibacterial activities of magnesium oxide (MgO) nanoparticles against foodborne pathogens. Journal of Nanoparticle Research 2011; 13: 6877–6885. doi: 10.1007/s11051-011-0595-5.

53. Singariya P, Kumar P, Mouriya KK. Antimicrobial activity of fruit coat (calyx) of withania somnifera against some multi drug resistant microbes. International Journal of Biological & Pharmaceutical Research 2012; 3(2): 252–258.

54. Koka JA, Wani AH, Yaqub Bhat M. Evaluation of antifungal activity of magnesium oxide (MgO) and iron oxide (FeO) nanoparticles on rot causing fungi. Journal of Drug Delivery & Therapeutics 2019; 9(2-s): 173–178. doi: 10.22270/jddt.v9i2-s.2479.

55. Essien ER, Astasie VN, Okeafor AO, Nwude DO. Biogenic synthesis of magnesium oxide nanoparticles using *Manihot esculenta* (Crantz) leaf extract. International Nano Letters 2020; 10: 43–48. doi: 10.1007/s40089-019-00290-w.

56. Navalon S, Garcia H. Nanoparticles for catalysis. Nanomaterials 2016; 6(7): 123. doi: 10.3390/nano6070123.

57. Narendhran S, Manikandan M, Baby Shakila P. Antibacterial, antioxidant properties of *Solanum trilobatum* and sodium hydroxide-mediated magnesium oxide nanoparticles: A green chemistry approach. Bulletin of Materials Science 2019; 42: 133. doi: 10.1007/s12034-019-1811-7.

58. Patil UH, Gaikwad DK. Phytochemical screening and microbicidal activity of stem bark of *Pterocarpus marsupium*. International Journal of

Pharma Sciences and Research 2011; 2(1): 36–40.

59. Lin ST, Klabunde JK. Thermally activated magnesium oxide surface chemistry. Adsorption and decomposition of phosphorus compounds. Langmuir 1985; 1(5): 600–605. doi: 10.1021/la00065a015.

60. Ekerdt JG, Klabunde KJ, Shapley JR, *et al*. Surface chemistry of organophosphorus compounds. The Journal of Physcical Chemistry 1988; 92(22): 6182–6188. doi: 10.1021/j100333a005.

61. Stoimenov PK, Klinger RL, Marchin GL, Klabunde KJ. Metal oxide nanoparticles as bactericidal agents. Langmuir 2002; 18(17): 6679–6686. doi: 10.1021/la0202374.

62. Sundrarajan M, Suresh J, Gandhi RR. A comparative study on antibacterial properties of MgO nanoparticles prepared under different calcination temperature. Digest Journal of Nanomaterials and Biostructures 2012; 7(3): 983–989.